Unbiased Profiling of the Human Proinsulin Biosynthetic Interaction Network Reveals a Role for Peroxiredoxin 4 in Proinsulin Folding

Duc T. Tran,[1] Anita Pottekat,[2] Saiful A. Mir,[1] Salvatore Loguercio,[3] Insook Jang,[2] Alexandre Rosa Campos,[4] Kathleen M. Scully,[1] Reyhaneh Lahmy,[1] Ming Liu,[5,6] Peter Arvan,[5] William E. Balch,[3,7] Randal J. Kaufman,[2] and Pamela Itkin-Ansari[1,8]

The β-cell protein synthetic machinery is dedicated to the production of mature insulin, which requires the proper folding and trafficking of its precursor, proinsulin. The complete network of proteins that mediate proinsulin folding and advancement through the secretory pathway, however, remains poorly defined. Here we used affinity purification and mass spectrometry to identify, for the first time, the proinsulin biosynthetic interaction network in human islets. Stringent analysis established a central node of proinsulin interactions with endoplasmic reticulum (ER) folding factors, including chaperones and oxidoreductases, that is remarkably conserved in both sexes and across three ethnicities. The ER-localized peroxiredoxin PRDX4 was identified as a prominent proinsulin-interacting protein. In β-cells, gene silencing of PRDX4 rendered proinsulin susceptible to misfolding, particularly in response to oxidative stress, while exogenous PRDX4 improved proinsulin folding. Moreover, proinsulin misfolding induced by oxidative stress or high glucose was accompanied by sulfonylation of PRDX4, a modification known to inactivate peroxiredoxins. Notably, islets from patients with type 2 diabetes (T2D) exhibited significantly higher levels of sulfonylated PRDX4 than islets
from healthy individuals. In conclusion, we have generated the first reference map of the human proinsulin interactome to identify critical factors controlling insulin biosynthesis, β-cell function, and T2D.

It is estimated that 422 million adults are living with diabetes globally (1). β-Cell physiology is tightly linked to all forms of diabetes, and thus a better understanding of β-cell function is necessary to combat this disease.

The majority of the β-cell's protein synthetic machinery is dedicated to insulin biosynthesis, beginning with translocation of preproinsulin from the cytoplasm into the endoplasmic reticulum (ER) (2). Following cleavage of the signal peptide, proinsulin folding in the ER results in a three-dimensional structure stabilized by three intramolecular disulfide bonds (2). Only properly folded proinsulin molecules can transit from the ER to the Golgi apparatus. In the Golgi, proinsulin encounters zinc, further assembles into hexamers, and is finally transported to immature secretory granules, where processing enzymes proteolytically cleave proinsulin to mature insulin (and

[1]Development, Aging and Regeneration Program, Sanford Burnham Prebys Medical Discovery Institute, La Jolla, CA
[2]Degenerative Diseases Program, Sanford Burnham Prebys Medical Discovery Institute, La Jolla, CA
[3]Department of Molecular Medicine, Scripps Research, La Jolla, CA
[4]Sanford Burnham Prebys Medical Discovery Institute Proteomic Core, La Jolla, CA
[5]Division of Metabolism, Endocrinology, and Diabetes, University of Michigan Medical School, Ann Arbor, MI
[6]Department of Endocrinology and Metabolism, Tianjin Medical University, Tianjin, China
[7]Integrative Structural and Computational Biology, Scripps Research, La Jolla, CA
[8]Department of Pediatrics, University of California, San Diego, La Jolla, CA

Corresponding authors: Pamela Itkin-Ansari, pitkin@sbpdiscovery.org, and Randal J. Kaufman, rkaufman@sbpdiscovery.org

C-peptide) for release in response to elevated blood glucose (2).

Every second, 6,000 preproinsulin molecules per β-cell are delivered to the ER for folding assisted by chaperones, cochaperones, and oxidoreductases (3). The critical role of proper folding in proinsulin biosynthesis is exemplified by rare heterozygous mutations in proinsulin that prevent correct disulfide bond formation (2). The misfolded proinsulin molecules resulting from a single mutant allele act in a dominant-negative fashion to entrap wild-type (WT) proinsulin in the ER, causing mutant *INS* gene–induced diabetes of youth (MIDY) in both humans and animal models (2).

Type 1 and type 2 (T2D) diabetes are typically associated with inflammation or oxidative stress, which may contribute to proinsulin misfolding and thereby limit the size of the properly folded proinsulin population (2,4). Moreover, we recently showed that even in healthy human islets, a portion of proinsulin is misfolded, suggesting that β-cells function near the limit of their capacity to produce properly folded proinsulin (4).

Misfolded proinsulin activates the unfolded protein response (UPR) signaled through two protein kinases, PERK and IRE1, and the transcription factor ATF6 (5) to help maintain cell proteostasis (6,7). The chaperone BiP (HSPA5) is both a target and an essential regulator of the UPR. Early in progression to diabetes, the three branches of the UPR adapt the β-cell's ER to prevent further accumulation of misfolded proinsulin. This is accomplished by *1*) attenuating proinsulin synthesis, *2*) inducing expression of genes that promote translocation, folding, and trafficking in the ER, and/or *3*) activating genes that are involved in elimination of misfolded proinsulin through ER-associated protein degradation (5). Studies demonstrate that UPR signaling is essential to preserve β-cell function and survival and that if the UPR fails to restore proper proinsulin folding, β-cells undergo apoptosis (8,9).

We recently showed that proinsulin misfolding in human islets is exacerbated by inhibition of the UPR factor PERK or of BiP (4), further highlighting the delicate nature of β-cell homeostasis. Indeed, defects anywhere in the biosynthetic network (folding, processing, trafficking, and exocytosis) can also lead to fulminant β-cell failure (10,11). Therefore, it is critical to understand the cellular components that promote human β-cell insulin homeostasis and how they are maintained in the presence of extracellular insults (12). Proteomic analyses have cataloged the proteins in human islets (13–16), but these global analyses do not distinguish which proteins reside in β-cells or define the proteins that physically interact with proinsulin to direct its folding and maturation.

Here, we used an unbiased affinity purification mass spectrometry (AP-MS) approach to identify the central machinery responsible for proinsulin production in human β-cells. The data reveal a rich proinsulin biosynthetic network that is remarkably conserved across a diverse group of donors. Further investigation of the network highlights a functional role for PRDX4 in promoting proinsulin folding that, importantly, may contribute to protection against T2D. Thus, the AP-MS data provide a roadmap for functional dissection of the proinsulin biosynthetic network and its impact on β-cell health.

RESEARCH DESIGN AND METHODS

Cell Culture
Human islets were cultured in Prodo Islet Complete Media (5.8 mmol/L glucose) (Prodo Laboratories). MIN6 cells were cultured in DMEM with 4.5 g/L glucose and L-glutamine, 0.34% sodium bicarbonate, 1× penicillin, streptomycin, 275 nmol/L β-mercaptoethanol, and 15% FBS. Human embryonic kidney (HEK) 293A and 293T cells were cultured in DMEM with 4.5 g/L glucose and L-glutamine, sodium pyruvate, 1× penicillin, streptomycin, and 10% FBS.

Proinsulin AP-MS
Normal islets (2,500 human islet equivalents) lysed in 50 mmol/L Tris, pH 7.4, 150 mmol/L NaCl and 1% TX-100, and 1× protease inhibitor cocktail (Thermo Fisher Scientific) were precleared with protein G agarose beads and then immunoprecipitated with beads cross-linked to mouse IgG or proinsulin antibody (20G11) overnight at 4°C. A sample of beads was removed for Western blot, and the majority of beads were processed for two-dimensional (2D) liquid chromatography–tandem mass spectrometry (LC-MS/MS) analysis.

Immunoprecipitated proteins were subjected to denaturation in 8 mol/L urea in 50 mmol/L ammonium bicarbonate buffer, reduced with Tris (2-carboxyethyl)phosphine, and alkylated with iodoacetamide. Urea concentration was diluted to 1 mol/L using 50 mmol/L ammonium bicarbonate, and samples were digested overnight with mass spectrometry (MS)-grade trypsin/Lys-C mix (Promega, Madison, WI). Digested proteins were finally desalted using a C18 TopTip (PolyLC, Columbia, MD) before subjection to LC-MS/MS analysis. To label samples with tandem mass tag (TMT), we used a TMTsixplex Isobaric Label kit (Thermo Fisher Scientific) according to manufacturer protocol.

Samples were analyzed by 2D LC-MS/MS using a 2D nanoACQUITY UltraPerformance Liquid Chromatography system (Waters Corp., Milford, MA) coupled to an Orbitrap Velos Pro mass spectrometer (Thermo Fisher Scientific). Peptides were loaded onto the first-dimension column, XBridge BEH130 C18 NanoEase (300 μm × 50 mm, 5 μm), equilibrated with solvent A (20 mmol/L ammonium formate, pH 10) at 2 μL/min. The first fraction was eluted from the first-dimension column at 17% of solvent B (100% acetonitrile) for 4 min and transferred to the second-dimension Symmetry C18 trap column (0.180 × 20 mm; Waters Corp.) using a 1:10 dilution with 99.9% 2D pump solvent A (0.1% formic acid in water) at 20 μL/min. Peptides were then eluted from the trap column and resolved on the analytical C18 BEH130 PicoChip column (0.075 × 100 mm, 1.7 μm particles; New Objective, Woburn, MA) at low pH by increasing the

composition of solvent B (100% acetonitrile) from 2% to 26% over 94 min at 400 nL/min. Subsequent fractions from the first-dimension fractions were eluted at 19.5%, 22%, 26%, and 65% solvent B and analyzed in a similar manner. The mass spectrometer was operated in positive data-dependent acquisition mode with up to five MS2 spectra triggered per duty cycle.

MS/MS spectra were searched against the *Homo sapiens* UniProt protein sequence database (January 2015 version) using MaxQuant (version 1.5.5.1) with false discovery rate (FDR) set to 1%. (Note proinsulin was searched as insulin.) Label-free (LF) intensity was normalized by Loess method using Normalyzer (17). MSstats was used to calculate a confidence (*P* value) and fold change of proinsulin immunoprecipitation (IP)–to–control IgG IP intensity ratio for each protein (18). All data including *.raw data file and MaxQuant *.txt search results are available online at ProteomeXchange (data set identifier PXD014476) (http://proteomecentral.proteomexchange.org/cgi/GetDataset).

Human islet lysates were similarly immunoprecipitated for proinsulin for validation studies. Bound proteins were eluted with 2× Laemmi buffer prior to Western blot analysis. MYC-tagged proinsulin and FLAG-tagged PRDX4 in HEK cells were immunoprecipitated with anti-MYC and anti-FLAG magnetic beads according to manufacturer protocol (Pierce).

Transfection

Plasmid expressing human PRDX4-FLAG was purchased from Sino Biological Inc. Vectors expressing WT or Akita mutant MYC-tagged human proinsulin were generated in the laboratory of P.A. (19). WT-PRDX4 pCDNA3.1 and C245A pCDNA 3.1 were a kind gift from Dr. Bulleid (Institute of Molecular Cell and Systems Biology, University of Glasgow, Scotland, U.K.) (20). pCDNA3.1 or GFP-PGK vectors were used as controls. Equal amounts of total DNA were transfected using ViaFect (Promega) or Lipofectamine (Thermo Fisher Scientific) transfection reagent following manufacturer instructions.

Western Blotting

Samples were prepared in 2× Laemmli sample buffer without (nonreducing) or with (reducing) 2.5% β-mercaptoethanol, boiled (100°C, 10 min), analyzed by SDS-PAGE, and transferred to nitrocellulose membranes. Membranes were blocked and incubated with corresponding primary antibodies (4°C, ON), rabbit BiP (for human islets), rabbit GRP94 (Cell Signaling Technology), rabbit ERDJ5, rabbit Myo18A (Proteintech), goat PRDX4 (R&D Systems), rabbit PRDX4 directly conjugated to horseradish peroxidase (PRDX4-HRP; LSBio), rabbit PRDX-SO$_3$, and MYC tag (Abcam) and, for mouse β-cells, rabbit vinculin (Proteintech), mouse proinsulin (HyTest Ltd.), mouse insulin antibody (a gift from P.A.), and rabbit BiP (a kind gift from Dr. Hendershot [St. Jude Children's Research Hospital, Memphis, TN]); for secondary antibodies, goat anti-mouse, goat anti-rabbit, donkey anti-goat, and donkey anti–guinea pig antibodies

were used in 1:5,000 (IRDye 800CW or IRDye 680RD; LI-COR Biosciences). Signals were visualized with LI-COR Odyssey CLx, and Western blot images were quantified by ImageJ. A detailed antibody list can be found in Supplementary Table 1.

PRDX4 Knockdown

Virus from retroviral vectors expressing GFP and shRNA targeting murine PRDX4 (OriGene Technologies, Rockville, MD) or nonspecific scramble control were used to infect MIN6 cells. Infected cells were selected by FACS sorting for high-GFP intensity.

Quantitative PCR Analysis

RNA was extracted using RNeasy kit (QIAGEN); and cDNAs were prepared using qScript cDNA SuperMix (Quantabio). Quantitative (q)PCR was performed with SYBR Green I analyzed by a LightCycler 96 (Roche Molecular Systems). Each gene was normalized to 18S. Primers: 18S (CCA GAGC GAAAGCATTTGCCAAGA/TCGGCATCGTTTATGGTCGGAACT), XBP1-T (AAG AACACGCTTGGGAATGG/ACTCCCCTTGGCCTC CAC), XBP1-S (GAGTCCGCAGGTG/GTGTCAGAGTCCATGGGA), AND PRDX4 (ACCAAGTATTTCCCACGATAGTC/GATCACTCC CTGCATCTAAGC).

Glucose-Stimulated Insulin Secretion

Glucose-stimulated insulin secretion was measured using mouse insulin and ultrasensitive human insulin ELISA kits (Mercodia) according to manufacture recommendations.

Data and Resource Availability

The data sets generated and analyzed in the current study are available in the ProteomeXchange repository (data set identifier PXD014476) (http://proteomecentral.proteomexchange.org/cgi/GetDataset) and at NDEx (https://public.ndexbio.org/#/network/0c0a451c-88b1-11ea-aaef-0ac135e8bacf).

RESULTS

Defining the Human Proinsulin Biosynthetic Interaction Network

To identify the physical interactions that dictate proper proinsulin biosynthesis, we first generated a series of monoclonal antibodies to human proinsulin. We chose a conformation-specific monoclonal antibody that selectively recognizes human proinsulin by IP (20G11) in the presence of 1% Triton X-100, with negligible cross-reactivity to mature insulin (Supplementary Fig. 1*A*). Because we recently found that even healthy islets harbor a subset of proinsulin molecules that are misfolded, we tested whether 20G11 recognizes misfolded human proinsulin in addition to the properly folded proinsulin. COS1 cells were transfected with WT human proinsulin or proinsulin variants bearing point mutations that cause severe misfolding leading to MIDY (21). 20G11 efficiently immunoprecipitated WT as well as all MIDY proinsulin mutants tested (Supplementary Fig. 1*B*). Therefore, we affinity purified proinsulin from human islets using 20G11 or control

mouse IgG for mass spectrometry (AP-MS). Notably, IP of proinsulin provided β-cell specificity in the context of intact islets, avoiding the need for islet dispersal or β-cell purification methods that can stress β-cells.

Initially, two MS quantification methodologies were compared: LF and TMT isobaric labeling approaches (Supplementary Fig. 2). Numerous interactors were similarly identified with both methods, but the dynamic range of fold change proinsulin IP versus IgG IP detected by TMT was compressed, relative to LF, as previously described (22). Therefore, LF was used for subsequent studies.

With the goal of identifying highly conserved proinsulin interactions at the core of normal human β-cell function, we procured islet preparations from six donors, including Caucasian, Hispanic, and African American ethnicities as well as both sexes. The donors had no history of diabetes and had BMI ranging from 21 to 25.4 kg/m^2 and normal HbA$_{1c}$ (4.8%–5.5%) at the time of death (Fig. 1A). Equal numbers of islet equivalents were lysed and immunoprecipitated with either 20G11 or mouse IgG–conjugated beads and subjected to on-bead denaturation, reduction, and trypsin digestion prior to LC-MS/MS analyses.

MS/MS spectra were searched against the human UniProt database and analyzed with MaxQuant. For statistical analyses, MSstats (18) was used to calculate a confidence score (P value) for each protein based on the reproducibility of detection across samples. Comparison of MS/MS counts for proinsulin (bait) across the six islet samples revealed remarkable consistency in the recovery of proinsulin, suggesting little biological or technical variability (Fig. 1B). Similarly, the profile of prey proteins coprecipitated with proinsulin (FDR <1%) was highly consistent across the samples (Fig. 1C).

For identification of the most robust proinsulin interactions for network analysis, the data were stringently filtered using the following criteria: 1) proinsulin IP–to–control IgG IP intensity ratios greater than or equal to twofold (log$_2$FC ≥1), 2) $P \leq 0.05$, and 3) total MS/MS across six samples ≥10. Moreover, for certainty that identified interactors were derived from β-cells, proteins were removed from analysis if their average mRNA expression in β-cells did not reach a minimum threshold of 1 count per million (CPM) as reported in a recent single-cell RNA-sequencing study in human islets (23). The resulting data set identified 461 proteins. These interactors were assigned to subcellular compartment or function, e.g., ER, using the Human Protein Atlas as the primary source for classification as well as manual curation (24) (Supplementary Table 2 and ProteomeXchange identifier PXD014476). For visualization of the network, nuclear, mitochondrial, and "undetermined" proteins were removed as previously described (25). Thus, we constructed the first human proinsulin biosynthetic network (Fig. 1D); increasing icon size represents significance (i.e., decreasing P value), and a thin line connects proinsulin to each interactor. Previously reported interactions among our identified proteins are depicted by gray lines, with line thickness

representing reported confidence score (26). An interactive map of Fig. 1D is also available: https://public.ndexbio.org/#/network/0c0a451c-88b1-11ea-aaef-0ac135e8bacf.

Known proinsulin interactors spanning the entire proinsulin biosynthetic pathway were identified, beginning with ribosomal proteins and the SEC61B translocon that transfers nascent proinsulin from the cytosol into the ER. At the distal end of the secretory pathway, we identified the proteolytic enzyme, PCSK1 (prohormone convertase 1), that cleaves the C-peptide/B chain junction of proinsulin. Given that enzyme interactions can be fleeting, identifying the proinsulin-PCSK1 association with high confidence ($P = 4.6 \times 10^{-5}$), demonstrates the sensitivity of the data. Conversely, the specificity of the affinity purification is highlighted by the absence of islet amyloid polypeptide (IAPP), a highly expressed β-cell protein that is stored and cosecreted with insulin but is not thought to interact physically with proinsulin in normal islets (27).

Among the novel proinsulin interactors we identified was the unconventional myosin-XVIIIa (MYO18A) ($P = 5.86 \times 10^{-6}$, log$_2$FC proinsulin IP–to–IgG IP intensity ratio 3.71), validated in Supplementary Fig. 3A. MYO18A links Golgi membranes to the cytoskeleton, likely participating in the tensile force required for vesicle budding from the Golgi (28). Therefore, our finding that MYO18A interacts with proinsulin, even if indirectly, supports the idea that there is specific recruitment of proinsulin (that withstands 1% Triton X-100) at the luminal aspect of budding Golgi membranes, as previously suggested (29).

ER Localized Folding Factors that Interact with Proinsulin

To identify the signaling pathways at the core of the data set, we applied Ingenuity Pathway Analysis (Fig. 2A). UPR, the most enriched pathway, and related categories, e.g., EIF2 signaling, were comprised mainly of chaperones and cochaperones. Signaling pathways that initially appeared as unusual, e.g., aldosterone, were in fact also composed of these factors (30). To capture ER folding factors that may interact transiently or only with a misfolded subset of the larger population of proinsulin molecules, we relaxed stringency, using $P \leq 0.05$ and β-cell expression criteria (Supplementary Table 3). The identified ER folding factor subnetwork is shown in Fig. 2B, where icon size represents log$_2$FC proinsulin IP–to–control IgG IP intensity ratio and line thickness represents increasing significance (i.e., decreasing P value).

Among the ER localized interactors were proteins we previously showed play essential roles in proinsulin folding or β-cell health, e.g., BiP/HSPA5, GRP94/HSP90B1 ERDJ6 (DNAJC3/p58^{IPK}), and PDIA1/P4HB (4,31–33) and novel factors like quiescin sulfhydryl oxidase 1 (QSOX1), an enzyme with no previously known substrates (34). The most robust proinsulin interaction (Log$_2$FC proinsulin IP–to–IgG IP intensity ratio 6.17, $P = 4.92 \times 10^{-11}$) was with thioredoxin-dependent peroxiredoxin 4 (PRDX4) a 2-cysteine peroxiredoxin that uses luminal H$_2$O$_2$ to oxidize
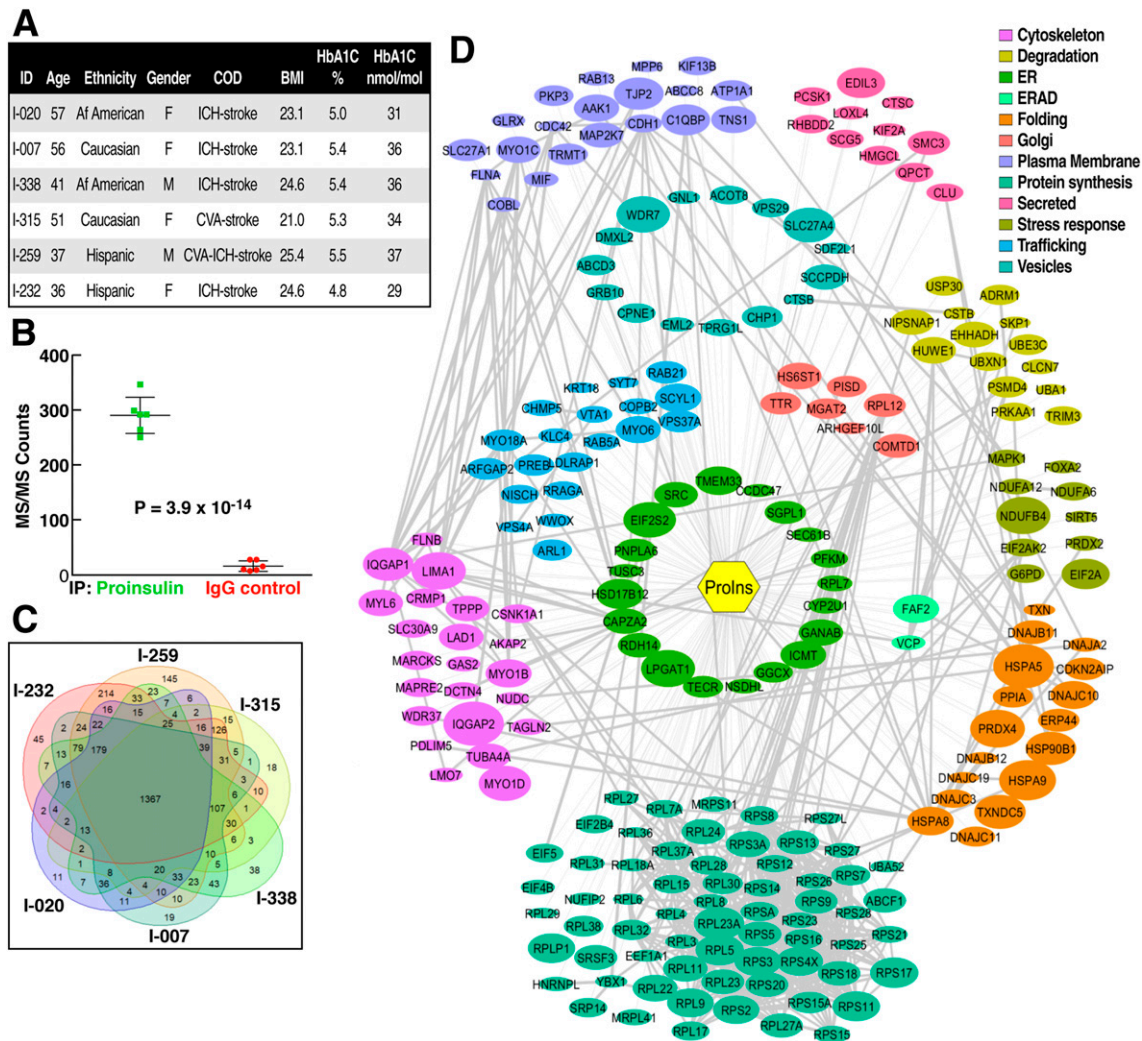
Figure 1—Defining the proinsulin biosynthetic interaction network. *A*: Human islets from six donors with no history of diabetes and with normal HbA$_{1c}$ were used for final AP-MS studies. Age is presented in years. *B*: Total MS/MS counts for proinsulin (bait) in the proinsulin IP or IgG IP from the six islet preparations reported in *A*. *C*: Venn diagram showing shared and unique proinsulin-interacting proteins identified with FDR ≤1% in the six islet preparations. *D*: Network analysis of robust proinsulin protein-protein interactions generated by Cytoscape. Data were filtered using all of the following criteria: *1*) proinsulin IP–to–control IP intensity ratios greater than or equal to twofold, *2*) *P* ≤ 0.05, *3*) total MS/MS across six samples ≥10, and *4*) mRNA expression in single-cell mRNA profiling of β-cells of at least 1 CPM (23). Protein categories defined by the Human Protein Atlas (24). For simplicity, interacting proteins in the categories nucleus and mitochondria, as well as those of the undetermined category, are not visualized in this figure but are included in uploaded analysis. Increasing icon size depicts increasing significance. Gray lines depict previously reported protein-protein interactions, and line thickness reflects confidence score (26). Af American, African American; CVA, cerebrovascular accident; ERAD, endoplasmic reticulum—associated protein degradation; F, female; ICH, intracerebral hemorrhage; ID, identifier; M, male; ProIns, proinsulin.

proteins (25) (Fig. 2*B* and Supplementary Fig. 3*B*). A recent single-cell RNA-sequencing study determined the expression level of PRDX4 specifically in human β-cells, shown relative to the β-cell transcription factor PDX1 and insulin in Supplementary Fig. 4 (23).

Functional Characterization of PRDX4 Suggests a Role in Proper Proinsulin Folding
PRDX4 peroxidase activity relies on a peroxidatic cysteine residue oxidized by luminal H$_2$O$_2$ to sulfenic acid, which then forms a disulfide bond with the resolving cysteine on an adjacent PRDX4 molecule. Thus, PRDX4 enzymatic activity requires dimerization or higher-order structures

(25). To investigate the conformational composition of PRDX4 in islets, we used nonreducing SDS-PAGE of murine islets. Virtually all PRDX4 protein was found in disulfide-linked dimers (at ~52 kDa) and high–molecular weight (HMW) complexes, with only a small fraction as the 28 kDa monomer (Fig. 2*C*, left lane). Importantly, the HMW PRDX4-containing complexes clearly involve additional proteins, as not all bands are multimers of 28 kDa. For validation of the specificity of the PRDX4 complexes, live islets were treated with increasing concentrations of dithiothreitol (DTT) (a reducing agent). High-DTT conditions resolved HMW PRDX4 species to monomer and the particularly stable dimer 52 kDa band (35) without
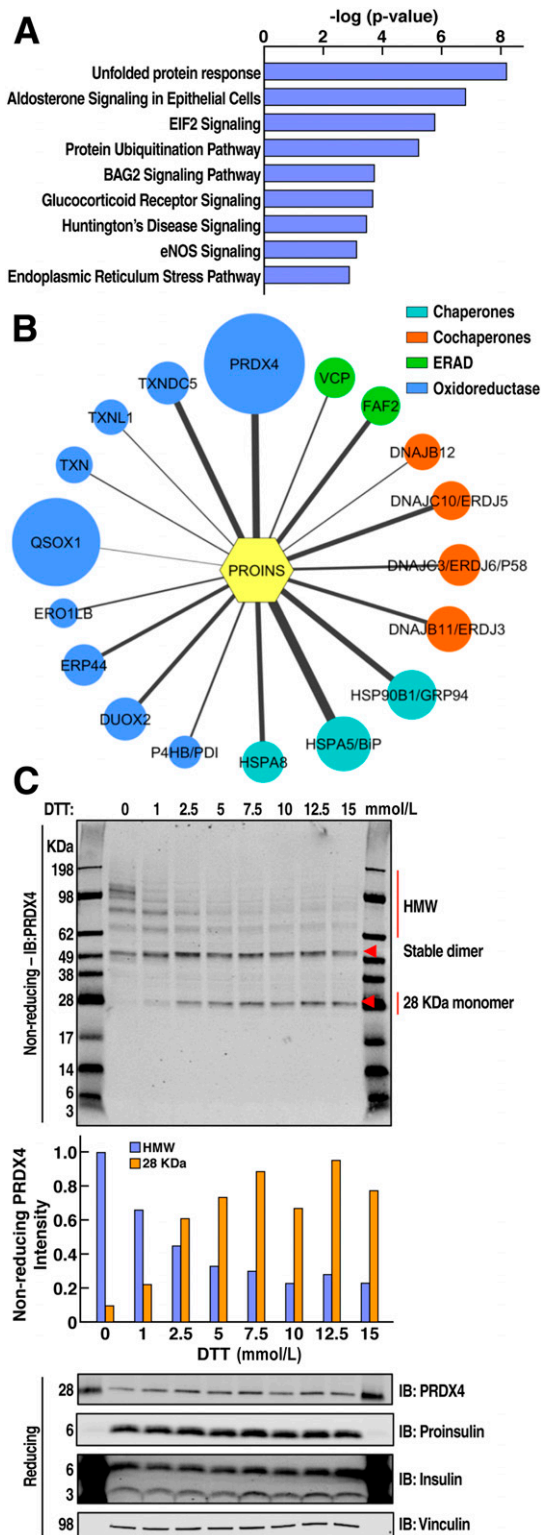
affecting the overall PRDX4 expression or expression of proinsulin and insulin. The data indicate that the complexes specifically contain PRDX4 and suggest that PRDX4 interactions with additional proteins occur via disulfide bonds.

For determination of whether PRDX4 interacts with both WT and misfolded proinsulin, HEK293 cells were cotransfected with plasmids expressing human PRDX4 and either WT or MIDY *Akita* mutant human proinsulin. The *Akita* mutation in the cysteine at A7 (C(A7)Y) leaves the B7 cysteine without its disulfide pairing partner required for proinsulin folding (2). IP of WT or Akita proinsulin coprecipitated PRDX4, revealing that PRDX4 interacts with both folded and misfolded proinsulin (Supplementary Fig. 3*C*). Conversely, PRDX4 IP from similarly prepared samples coimmunoprecipitated both WT and Akita proinsulin (Supplementary Fig. 3*C*).

Given the importance of BiP to proinsulin folding, we asked whether proinsulin-PRDX4 interactions required BiP. HEK cells transfected with PRDX4 and human proinsulin were treated with the BiP ATPase inhibitor HA15, the Shiga-toxic *Escherichia coli* virulence factor subtilase cytotoxin (SubAB) that cleaves and inactivates BiP (36), or mutant SubAB, an enzymatically inactive form of SubAB (Fig. 3*A*). IP of PRDX4 coimmunoprecipitated proinsulin independent of BiP inhibition or cleavage, indicating that intact or enzymatically active BiP is not required for proinsulin-PRDX4 interactions (Fig. 3*A*). These experiments further revealed that PRDX4 interacts physically with BiP in both the presence and absence of proinsulin (Fig. 3*B*). Controls showed that all PRDX4 conformations were immunoprecipitated and that proinsulin and BiP did not bind to beads nonspecifically (Supplementary Fig. 5*A* and *B*). Thus, PRDX4 binds to proinsulin independent of BiP and PRDX4 binds to BiP independent of proinsulin.

To determine whether proinsulin folding is assisted by PRDX4, lentiviral vectors expressing shRNA were used to deplete PRDX4 in MIN6 cells, achieving 64%–75% PRDX4 knockdown compared with controls (Fig. 4*A* and *B*). PRDX4 knockdown triggered modest proinsulin misfolding as revealed by an increase of HMW complexes. Moreover, PRDX4-depleted MIN6 cells were hypersensitive to proinsulin misfolding induced by oxidant challenge with 10 μmol/L menadione (31) or 1 mmol/L H_2O_2 for 1 h (Fig. 4*A*). We similarly observed that menadione-induced oxidative stress caused proinsulin misfolding in human islets (Supplementary Fig. 6). Of note, proinsulin misfolding was accompanied by conformational changes of PRDX4 into

Figure 2—Human proinsulin interacts with ER resident folding factors, including PRDX4. *A*: Ingenuity Pathway Analysis of identified proinsulin interactors (not included are mitochondrial and ribosomal proteins) reveals enrichment of UPR as a major pathway involved in proinsulin biosynthesis. *B*: Proinsulin-interacting ER resident folding factors with *P* value ≤0.05. Icon size reflects $\log_2$FC proinsulin IP–to–IgG IP intensity ratio, and line thickness represents increasing significance (decreasing *P* values). *C*: PRDX4 conformational analysis in normal murine islets. Live islets treated with a gradient of DTT concentrations ranging from 1 to 15 mmol/L for 20 min (or untreated

control [0], left lane) were lysed and resolved by nonreducing SDS-PAGE immunoblotted (IB) for PRDX4 and by reducing SDS-PAGE immunoblotted for PRDX4, proinsulin, insulin, and vinculin. Intensity of disulfide-linked HMW complexes (49–198 kDa) versus PRDX4 monomer (28 kDa) is quantified in graph. Molecular weight markers are shown. ERAD, endoplasmic reticulum—associated protein degradation; PROINS, proinsulin.
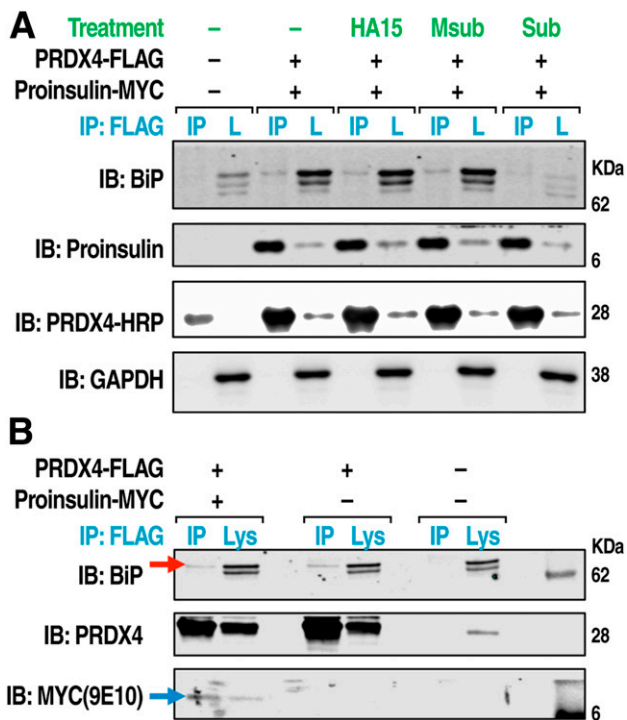
Figure 3—PRDX4 interacts with proinsulin and BiP, and these interactions are independent of each other. *A*: HEK 293T cells were transfected with plasmids expressing human proinsulin-MYC and human PRDX4-FLAG or untransfected. After 44 h, cells were treated with SubAb that cleaves BiP (Sub) (2 μg/mL, 4 h), mutant SubAb as control (Msub) (2 μg/mL, 4 h), or the BiP inhibitor HA15 (10 μmol/L, 4 h) or untreated, followed by cell lysis and IP with anti-FLAG magnetic beads. Three percent of lysate (L) and 20% of immunoprecipitate were analyzed on reducing SDS-PAGE. Note: antibody light-chain band appears just below PRDX4. *B*: HEK 293A cells were transfected with equal amounts of total plasmid in combination of control pCDNA (−), human proinsulin-MYC, and human PRDX4-FLAG. Resulting lysates were subject to IP with anti-FLAG magnetic beads. Lysates and IP fractions were immunoblotted (IB) for BiP, PRDX4, or MYC tag (proinsulin). Red arrow identifies BiP, and blue arrow identifies proinsulin-MYC band. Lys, lysate.

HMW disulfide-bonded complexes, suggesting that PRDX4 may be recruited to client proteins during oxidative stress.

We considered that decreased PRDX4 expression might activate the UPR. mRNA expression levels of the factors BiP, PDIA1, and CHOP were not altered by low PRDX4 expression (data not shown). We found, however, that reduced expression of PRDX4 decreased the ratio of the IRE1 target spliced X-box binding protein 1 (37) (XBP1s) mRNA, relative to total XBP1 (XBP1t), which was surprising, warranting future investigation of UPR (Fig. 4*B*).

We next asked whether increased expression of PRDX4 could promote proper proinsulin folding. HEK 293 cells were cotransfected with WT human proinsulin and control plasmid, WT PRDX4, or a mutant form of PRDX4 (C245A) that lacks enzymatic activity (20) (Fig. 4*C*). Exogenous WT PRDX4 decreased HMW proinsulin species (>28 kDa) relative to controls, while the C245A mutant PRDX4 did not (Fig. 4*C*), suggesting that PRDX4 oxidoreductase

activity is required to promote proinsulin folding. Both WT and mutant PRDX4 induced BiP expression, but the finding that only WT PRDX4 promoted proinsulin folding indicates that BiP upregulation alone was not responsible for improved proinsulin folding by WT PRDX4.

The expression of multiple ER proteins increases in response to glucose stimulation of β-cells (37); we therefore probed whether PRDX4 expression was glucose responsive (Fig. 5*A*). In MIN6 cells, high-glucose treatment overnight resulted in a 3.3-fold increase in secreted insulin, accompanied by a 73% increase in intracellular steady-state levels of proinsulin but no change in PRDX4 expression (Fig. 5*A*). Nonreducing SDS-PAGE analysis of proinsulin showed that the ratio of misfolded to properly folded remained constant in high-glucose conditions.

Under high H_2O_2 conditions, the peroxidactic cysteine of PRDX4 can become irreversibly overoxidized to sulfonic acid (PRDX4-SO$_3$) (referred to as sulfonylation), which inactivates PRDX4 enzymatic activity (38). We therefore investigated the effect of high glucose on PRDX4 sulfonylation in MIN6 cells, finding that high glucose significantly increased sulfonylated PRDX4 relative to total PRDX4 (Fig. 5*A*).

We next examined the effects of high glucose on proinsulin folding and PRDX4 in human islets. Similar to MIN6 cells, high glucose stimulated insulin release into the media (Fig. 5*B*), a significant increase in the steady-state level of intracellular proinsulin, and no change in PRDX4 expression. In human islets, glucose induced a 2.3-fold increase in BiP in response to glucose. Notably, nonreducing SDS-PAGE revealed that high glucose increased the fraction of proinsulin that was misfolded in human islets (Fig. 5*B*). In contrast to MIN6 cells, normal human islets treated overnight with high glucose did not exhibit PRDX4 sulfonylation.

We considered that the difference in PRDX4 status between MIN6 and human islets might be due to normoglycemic in vivo conditions for the human islets versus long-term culture of MIN6 cells in high-glucose media. This prompted us to ask whether chronic high glucose in human T2D might induce PRDX4 sulfonylation. Indeed, examination of a series of human islet samples from patients with T2D ($n = 4$, HbA$_{1c}$ 6.5%–8.5% or 48–69 mmol/mol) versus healthy individuals ($n = 4$, HbA$_{1c}$ 4.2%–5.9% or 22–41 mmol/mol) revealed for the first time that the fraction of sulfonylated PRDX4 in islets is elevated in T2D (3.3-fold, $P = 0.011$) (Fig. 6). Thus, PRDX4 appears to be selectively inactivated in islets from patients with T2D.

DISCUSSION

Here we provide the first reference map of human proinsulin's transit through the biosynthetic pathway. The most striking feature of this data set is the tight conservation of the human proinsulin biosynthetic network across six donors reflecting three ethnicities and both sexes. A technical aspect that may have contributed to the data
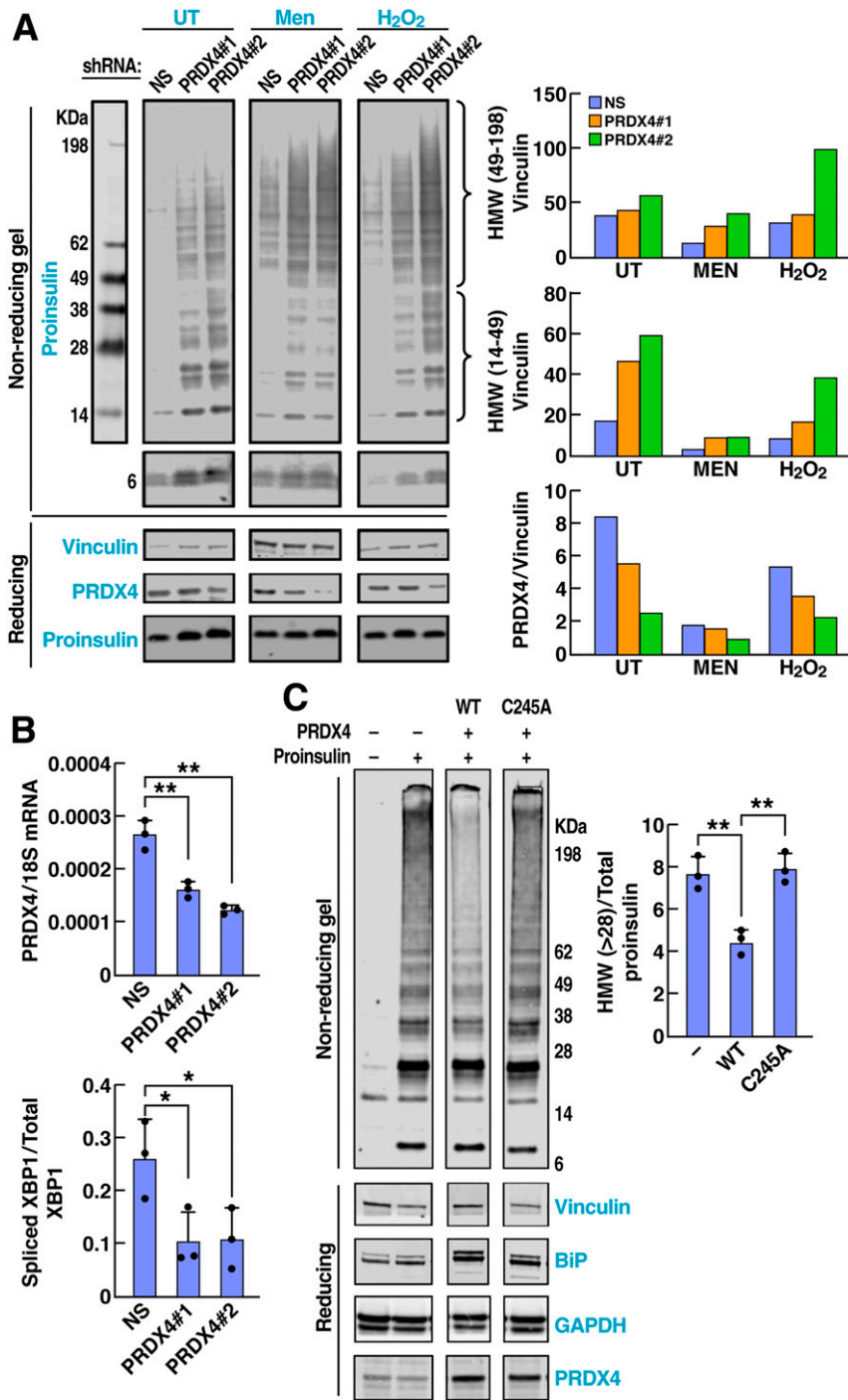
Figure 4—PRDX4 facilitates proinsulin folding. *A*: Loss of PRDX4 increases proinsulin misfolding. PRDX4 was knocked down in MIN6 cells by stable expression of PRDX4 shRNA (PRDX4#1 and PRDX4#2) or scrambled nonspecific shRNA (NS). Cells were untreated (UT) or treated with the oxidant menadione (Men) (100 μmol/L, 1 h) or H_2O_2 (1 mmol/L, 1 h). Nonreducing gels were immunoblotted with proinsulin antibody CCI17. Bottom panels of nonreducing gel show darker exposure of proinsulin monomer band at ~6 kDa. Reducing gels were immunoblotted for vinculin, PRDX4, and total proinsulin. Accompanying graphs (right) show quantification of HMW proinsulin bands from 14 to 49 kDa or 49 to 198 kDa from nonreducing gel and total PRDX4 from reducing gel, normalized by vinculin. The data are representative of four independent experiments. *B*: mRNA derived from cells described in *A* confirms PRDX4 knockdown in MIN6 stably expressed PRDX4 shRNA by qPCR using three biological replicates per line. Lower panel: qPCR analysis of the ER stress marker spliced XBP1(s) relative to total XBP1(t). *C*: HEK 293T cells were transfected with equal amounts of plasmid containing combinations of human proinsulin-MYC, human WT-PRDX4, and human PRDX4 harboring a mutation in the resolving cysteine (C245A-PRDX4) and GFP or untransfected. Resulting lysates were analyzed by nonreducing and reducing SDS-PAGE. Accompanying graph shows ratios of disulfide-bonded HMW complexes (molecular weight >28) to corresponding total proinsulin intensity determined on reducing gel. **$P < 0.01$.
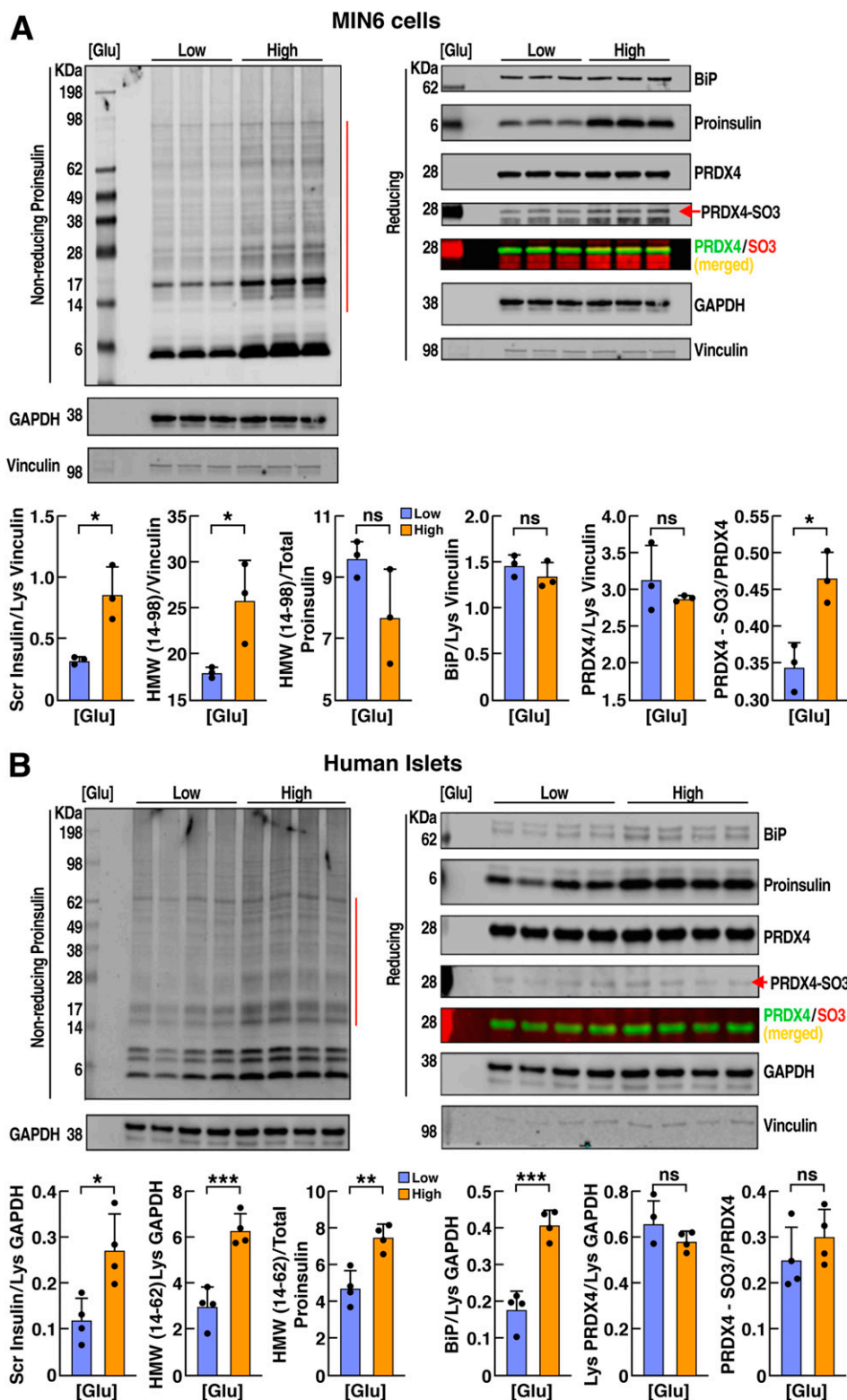
Figure 5—Analysis of high glucose–induced proinsulin misfolding and PRDX4 expression in MIN6 and human islets. *A*: MIN6 cells were glucose starved for 1 h and then treated with low (2.2 mmol/L, $n = 3$) or high (22 mmol/L, $n = 3$) glucose (Glu) for 22.5 h. HMW proinsulin complexes (red bar) were resolved on nonreducing SDS-PAGE. Samples were also analyzed on reducing SDS-PAGE and immunoblotted for BiP, total proinsulin, PRDX4, and PRDX-SO$_3$ along with loading controls (vinculin and GAPDH). PRDX4 and PRDX-SO$_3$ were immunoblotted with two different primary and secondary antibodies on the same membrane, and the images were merged. Red arrow shows PRDX4-SO$_3$ band identified by the PRDX-SO$_3$ antibody. Accompanying graphs show secreted (scr) insulin assayed by ELISA in the media relative to vinculin in lysate (Lys), HMW proinsulin complexes in lysate (red bar) to vinculin, HMW proinsulin complexes (red bar) in lysate to total proinsulin, BiP to vinculin, and total PRDX4 to vinculin and PRDX4-SO$_3$ band normalized to total PRDX4. *B*: Human islets were glucose starved for 1 h prior to treatment with low (3 mmol/L, $n = 4$) or high (30 mmol/L, $n = 4$) glucose for 18 h. HMW proinsulin complexes (red bar)
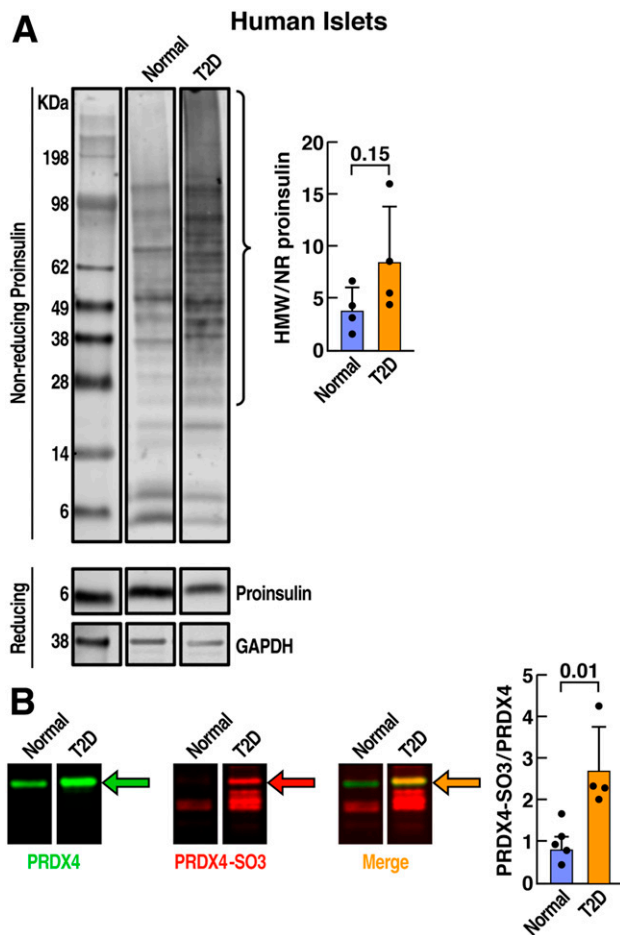
Figure 6—T2D islets exhibit increased PRDX4 sulfonylation. *A*: 8.55 μg protein from human islet preparations from four normal individuals and four patients with T2D was analyzed by nonreducing (NR) SDS-PAGE (upper panel) and immunoblotted for proinsulin (one representative sample is displayed here). The accompanying graph shows quantification of HMW bands (size range indicated by curved bracket) normalized by proinsulin monomer on the nonreducing gel for all eight samples. Reducing gels were immunoblotted for total proinsulin and GAPDH loading control (bottom panels). *B*: All samples were immunoblotted for both PRDX4 (green) and sulfonylated PRDXs (i.e., PRDX-SO$_3$ [red]) on the same membrane. Merged image shows colocalization of PRDX4 band with its sulfonylated version at the same molecular weight. Intensity of the sulfonylated PRDX4 bands (yellow arrow) versus total PRDX4 was quantified.

concordance was that human islets for AP-MS were procured from a single source to avoid artifacts resulting from site-specific islet isolation practices. We corroborate previously identified proinsulin-interacting proteins (9,31,32) and extend those studies to provide an entire interaction network.

We previously performed AP-MS to identify proinsulin and insulin interactors in murine MIN6 cells (39). Consistent with those studies, here we identified ERDJ3, DNAJC3/p58[IPK], and ERP44 as high-confidence human proinsulin-interacting proteins. Not surprisingly, TMEM24, which interacted more robustly with mature insulin than with proinsulin in MIN6 cells, was not identified in this study focused solely on proinsulin interactions in human islets.

Among the most significant newly identified proinsulin-interacting proteins was PRDX4. It will be of interest to determine whether the proinsulin-PRDX4 interaction is direct and the other potential members of the complex. One of these factors may well be BiP, which we showed binds to both proinsulin and PRDX4. It has also been suggested that clients of PRDX4 are PDI family members, e.g., PDIA1, which was also identified in our study (40).

In yeast, it has been suggested that the single PRDX-like protein is a molecular triage agent that absorbs oxidation (41). PRDX4 is not essential for survival in mice (42), but we find that proinsulin is more prone to misfolding when PRDX4 levels are low, particularly in cells stressed by oxidant treatment. The idea that PRDX4 may be required under stress conditions is consistent with the findings that mice lacking PRDX4 are more prone to lipopolysaccharide-induced toxicity (43) or to dextran sulfate sodium–induced colitis (44). Further, in mouse embryonic fibroblasts under normal conditions, loss of the oxidoreductase ERO1 (a proinsulin interactor identified here) renders the cells dependent on PRDX4 for growth (25) and in mouse hearts, loss of the oxidoreductase QSOX1, another of our identified proinsulin interactors, induces compensatory upregulation of PRDX4 (45). Together, our data and the work of others suggest that PRDX4 function may be redundant with other oxidoreductases under normal conditions but become critical under stress. Whether PRDX4 is required to buffer diabetogenic islet stress in vivo is an avenue for further investigation.

We show that overexpression of PRDX4 improves proinsulin folding. In accordance with this finding, others have observed that increased PRDX4 expression in INS1 cells improved glucose-induced insulin secretion (46) and, in mice, that overexpression of PRDX4 provided protection against streptozotocin-induced diabetes (47).

Excessive oxidation inactivates PRDX4 by sulfonylation, a two-step process. PRDX4 sulfenic acid is first modified to sulfinic acid, which may be the rate-limiting step. Further oxidation then results in irreversible sulfonylation (38). Acute high-glucose treatment induced PRDX4 sulfonylation in MIN6 cells, similar to a report in INS-1 cells (46),

were resolved on nonreducing SDS-PAGE. Samples were analyzed on reducing and nonreducing SDS-PAGE as described in *A*. Accompanying graphs are as described in *A* except that GAPDH is used to normalize secreted insulin, HMW proinsulin, and PRDX4 instead of vinculin.

but not in human islets. We hypothesize that chronic exposure of the MIN6 and INS-1 cells to high-glucose culture media may shift PRDX4 from sulfenic acid to sulfinic acid, poising PRDX4 for sulfonylation in those cells. In contrast, the human islets were procured from normoglycemic donors, where sulfenic acid may be the predominant form of PRDX4.

The idea that chronic high glucose predisposes PRDX4 to sulfonylation is consistent with our data showing increased PRDX4 sulfonylation in islets from patients with T2D. Notably, the proinsulin from these samples also exhibited a trend toward increased misfolding. Together, the data suggest that β-cells in patients with T2D have increased oxidative stress and/or diminished capacity to handle oxidative stress, which is in agreement with previous studies (48,49). PRDX4-SO_3 may in fact be a measure of the degree of oxidative stress in β-cells. PRDX4 can also be secreted and has been identified in extracellular vesicles (43). It is intriguing that serum samples from patients with T2D have higher levels of circulating PRDX4 than in control subjects (50). It is not yet known whether the circulating PRDX4 emanates from β-cells or whether the PRDX4 is modified by sulfonylation—questions with implications for diagnosing β-cell stress in a minimally invasive manner.

In summary, we have identified a complex network of factors that dictate proinsulin folding and trafficking through the exocytic pathway in human β-cells. The proinsulin interaction network provides a critical resource to characterize previously unknown molecular features of the β-cell secretory pathway and to determine their relevance in diabetes.

References

1. World Health Organization. Diabetes [Internet], 2020. Geneva, World Health Organization. Available from https://www.who.int/news-room/fact-sheets/detail/diabetes. Accessed 15 May 2020
2. Liu M, Weiss MA, Arunagiri A, et al. Biosynthesis, structure, and folding of the insulin precursor protein. Diabetes Obes Metab 2018;20(Suppl. 2):28–50
3. Schuit FC, Kiekens R, Pipeleers DG. Measuring the balance between insulin synthesis and insulin release. Biochem Biophys Res Commun 1991;178:1182–1187
4. Arunagiri A, Haataja L, Pottekat A, et al. Proinsulin misfolding is an early event in the progression to type 2 diabetes. eLife 2019;8:e44532
5. Scheuner D, Kaufman RJ. The unfolded protein response: a pathway that links insulin demand with β-cell failure and diabetes. Endocr Rev 2008;29:317–333
6. Hutt DM, Balch WE. Expanding proteostasis by membrane trafficking networks. Cold Spring Harb Perspect Biol 2013;5:a013383
7. Powers ET, Balch WE. Diversity in the origins of proteostasis networks–a driver for protein function in evolution. Nat Rev Mol Cell Biol 2013;14:237–248
8. Wu J, Kaufman RJ. From acute ER stress to physiological roles of the unfolded protein response. Cell Death Differ 2006;13:374–384
9. Scheuner D, Vander Mierde D, Song B, et al. Control of mRNA translation preserves endoplasmic reticulum function in beta cells and maintains glucose homeostasis. Nat Med 2005;11:757–764
10. Lu M, Lawrence DA, Marsters S, et al. Opposing unfolded-protein-response signals converge on death receptor 5 to control apoptosis. Science 2014;345:98–101
11. Roth DM, Hutt DM, Tong J, et al. Modulation of the maladaptive stress response to manage diseases of protein folding. PLoS Biol 2014;12:e1001998
12. Back SH, Kaufman RJ. Endoplasmic reticulum stress and type 2 diabetes. Annu Rev Biochem 2012;81:767–793
13. Waanders LF, Chwalek K, Monetti M, Kumar C, Lammert E, Mann M. Quantitative proteomic analysis of single pancreatic islets. Proc Natl Acad Sci U S A 2009;106:18902–18907
14. Ahmed M, Forsberg J, Bergsten P. Protein profiling of human pancreatic islets by two-dimensional gel electrophoresis and mass spectrometry. J Proteome Res 2005;4:931–940
15. Schrimpe-Rutledge AC, Fontès G, Gritsenko MA, et al. Discovery of novel glucose-regulated proteins in isolated human pancreatic islets using LC-MS/MS-based proteomics. J Proteome Res 2012;11:3520–3532
16. Zhang L, Lanzoni G, Battarra M, Inverardi L, Zhang Q. Proteomic profiling of human islets collected from frozen pancreata using laser capture microdissection. J Proteomics 2017;150:149–159
17. Chawade A, Alexandersson E, Levander F. Normalyzer: a tool for rapid evaluation of normalization methods for omics data sets. J Proteome Res 2014;13:3114–3120
18. Choi M, Chang C-Y, Clough T, et al. MSstats: an R package for statistical analysis of quantitative mass spectrometry-based proteomic experiments. Bioinformatics 2014;30:2524–2526
19. Liu M, Haataja L, Wright J, et al. Mutant INS-gene induced diabetes of youth: proinsulin cysteine residues impose dominant-negative inhibition on wild-type proinsulin transport. PLoS One 2010;5:e13333
20. Tavender TJ, Sheppard AM, Bulleid NJ. Peroxiredoxin IV is an endoplasmic reticulum-localized enzyme forming oligomeric complexes in human cells. Biochem J 2008;411:191–199
21. Liu M, Hodish I, Rhodes CJ, Arvan P. Proinsulin maturation, misfolding, and proteotoxicity. Proc Natl Acad Sci U S A 2007;104:15841–15846

22. Megger DA, Pott LL, Ahrens M, et al. Comparison of label-free and label-based strategies for proteome analysis of hepatoma cell lines. Biochim Biophys Acta 2014;1844:967–976

23. Wang YJ, Schug J, Won K-J, et al. Single-cell transcriptomics of the human endocrine pancreas. Diabetes 2016;65:3028–3038

24. Uhlén M, Fagerberg L, Hallström BM, et al. Proteomics. Tissue-based map of the human proteome. Science 2015;347:1260419

25. Zito E, Melo EP, Yang Y, Wahlander Å, Neubert TA, Ron D. Oxidative protein folding by an endoplasmic reticulum-localized peroxiredoxin. Mol Cell 2010;40:787–797

26. Alanis-Lobato G, Andrade-Navarro MA, Schaefer MH. HIPPIE v2.0: enhancing meaningfulness and reliability of protein-protein interaction networks. Nucleic Acids Res 2017;45:D408–D414

27. Knight JD, Williamson JA, Miranker AD. Interaction of membrane-bound islet amyloid polypeptide with soluble and crystalline insulin. Protein Sci 2008;17:1850–1856

28. Taft MH, Behrmann E, Munske-Weidemann L-C, Thiel C, Raunser S, Manstein DJ. Functional characterization of human myosin-18A and its interaction with F-actin and GOLPH3. J Biol Chem 2013;288:30029–30041

29. Orci L, Ravazzola M, Perrelet A. (Pro)insulin associates with Golgi membranes of pancreatic B cells. Proc Natl Acad Sci U S A 1984;81:6743–6746

30. Braakman I, Bulleid NJ. Protein folding and modification in the mammalian endoplasmic reticulum. Annu Rev Biochem 2011;80:71–99

31. Jang I, Pottekat A, Poothong J, et al. PDIA1/P4HB is required for efficient proinsulin maturation and ß cell health in response to diet induced obesity. eLife 2019;8:e44528

32. Ghiasi SM, Dahlby T, Hede Andersen C, et al. Endoplasmic reticulum chaperone glucose-regulated protein 94 is essential for proinsulin handling. Diabetes 2019;68:747–760

33. Han J, Song B, Kim J, et al. Antioxidants complement the requirement for protein chaperone function to maintain β-cell function and glucose homeostasis. Diabetes 2015;64:2892–2904

34. Rudolf J, Pringle MA, Bulleid NJ. Proteolytic processing of QSOX1A ensures efficient secretion of a potent disulfide catalyst. Biochem J 2013;454:181–190

35. Tavender TJ, Springate JJ, Bulleid NJ. Recycling of peroxiredoxin IV provides a novel pathway for disulfide formation in the endoplasmic reticulum. EMBO J 2010;29:4185–4197

36. Paton AW, Beddoe T, Thorpe CM, et al. AB5 subtilase cytotoxin inactivates the endoplasmic reticulum chaperone BiP. Nature 2006;443:548–552

37. Hassler JR, Scheuner DL, Wang S, et al. The IRE1α/XBP1s pathway is essential for the glucose response and protection of β cells. PLoS Biol 2015;13:e1002277

38. Wood ZA, Schröder E, Robin Harris J, Poole LB. Structure, mechanism and regulation of peroxiredoxins. Trends Biochem Sci 2003;28:32–40

39. Pottekat A, Becker S, Spencer KR, et al. Insulin biosynthetic interaction network component, TMEM24, facilitates insulin reserve pool release. Cell Rep 2013;4:921–930

40. Zito E. PRDX4, an endoplasmic reticulum-localized peroxiredoxin at the crossroads between enzymatic oxidative protein folding and nonenzymatic protein oxidation. Antioxid Redox Signal 2013;18:1666–1674

41. Day AM, Brown JD, Taylor SR, Rand JD, Morgan BA, Veal EA. Inactivation of a peroxiredoxin by hydrogen peroxide is critical for thioredoxin-mediated repair of oxidized proteins and cell survival. Mol Cell 2012;45:398–408

42. Iuchi Y, Okada F, Tsunoda S, et al. Peroxiredoxin 4 knockout results in elevated spermatogenic cell death via oxidative stress. Biochem J 2009;419:149–158

43. Lipinski S, Pfeuffer S, Arnold P, et al. Prdx4 limits caspase-1 activation and restricts inflammasome-mediated signaling by extracellular vesicles. EMBO J 2019;38:e101266

44. Takagi T, Homma T, Fujii J, et al. Elevated ER stress exacerbates dextran sulfate sodium-induced colitis in PRDX4-knockout mice. Free Radic Biol Med 2019;134:153–164

45. Caillard A, Sadoune M, Cescau A, et al. QSOX1, a novel actor of cardiac protection upon acute stress in mice. J Mol Cell Cardiol 2018;119:75–86

46. Mehmeti I, Lortz S, Elsner M, Lenzen S. Peroxiredoxin 4 improves insulin biosynthesis and glucose-induced insulin secretion in insulin-secreting INS-1E cells. J Biol Chem 2014;289:26904–26913

47. Ding Y, Yamada S, Wang K-Y, et al. Overexpression of peroxiredoxin 4 protects against high-dose streptozotocin-induced diabetes by suppressing oxidative stress and cytokines in transgenic mice. Antioxid Redox Signal 2010;13:1477–1490

48. Lupi R, Del Guerra S, Mancarella R, et al. Insulin secretion defects of human type 2 diabetic islets are corrected in vitro by a new reactive oxygen species scavenger. Diabetes Metab 2007;33:340–345

49. Ceriello A, Mercuri F, Quagliaro L, et al. Detection of nitrotyrosine in the diabetic plasma: evidence of oxidative stress. Diabetologia 2001;44:834–838

50. El Eter E, Al-Masri AA. Peroxiredoxin isoforms are associated with cardiovascular risk factors in type 2 diabetes mellitus. Braz J Med Biol Res 2015;48:465–469